buildings

MDPI

Article

Design of Prestressed Cable Dome Using Minor Perturbation Method

Haitao Zhou [1], Feng Fu [2,*], Bo Si [3], Deqing You [3] and Fengjian Zhang [4]

[1] School of Architecture and Art, Ningbo Polytechnic, Ningbo 315000, China; 2022057@nbpt.edu.cn
[2] Department of Engineering, School of Science and Technology, Northampton Square, University of London, London EC1VOHB, UK
[3] Beijing Building Construction Research Institute Co., Ltd., Beijing 100039, China; sibo-jgs@bbcri.bcegc.com (B.S.)
[4] School of Materials and Chemical Engineering, Henan University of Urban Construction, Pingdingshan 037500, China; 30010608@huuc.edn.cn
* Correspondence: feng.fu.1@city.ac.uk

Abstract: For the structural design of cable domes, the determination of prestress force distribution, the section of the structural components, and initial configuration are prerequisites for the subsequent detailed design of cable and strut sizes. To solve this problem, this paper elucidates the basic theory of the Minor Perturbation Method, introduces this theory into the field of force finding design for cable dome structures, and develops a new design method whose core is the comparison between the combined stress of each component conforming to mechanical characteristics of cable-strut structure and control stress, and meeting the convergence condition by adjusting the prestress level and cross-section of components. A corresponding design flow chart is established and programmed with finite element analysis software. Through the case studies of two different kinds of cable dome, it is proven that the proposed method and software program can simply, quickly, and effectively design the cable domes with an economic cross-section.

Keywords: cable dome; form-finding; force-finding; minor perturbation method

Academic Editor: Humberto Varum

Received: 29 November 2024
Revised: 24 December 2024
Accepted: 26 December 2024
Published: 31 December 2024

Citation: Zhou, H.; Fu, F.; Si, B.; You, D.; Zhang, F. Design of Prestressed Cable Dome Using Minor Perturbation Method. *Buildings* **2025**, *15*, 114. https://doi.org/10.3390/buildings15010114

1. Introduction

The cable dome structure belongs to the typical tensile structure system [1]. Conducting a feasible prestress design for cable dome structures is essential for their ability to resist loads and, therefore, determining the cross-sections area of each component and the overall initial geometry is important. These two design-stage structures are collectively referred to as form-finding and force-finding, or the prestress force design.

For the prestressing force design of tensile structures under given loads, but with uncertain geometry and prestressing distribution, the primary analysis methods are the force density method, the dynamic relaxation method, etc. [2,3]. In 1974, HJ Schek [4] proposed the method of force density by establishing node static equilibrium matrix equations in membrane structures. In 1988, L. Grundig [5] et al. enriched the applicable boundary range and node external force types based on the minimum area calculation theory. In 2006, JY Zhang et al. [6]. further studied the feasible force density set and the corresponding non-degenerate structural configuration. Hoang Chi Tran [7] et al. found feasible force density sets by iteratively performing the spectral decomposition of the force density matrix and singular value decomposition of the balance matrix. Masaaki Miki [8] and Metro R et al. contributed to the application methods and scope of the development

force density method a great deal. Metro R et al. [9] generalized the force density method to triangle planar elements, forming the surface density method [10].

Day [11] first proposed the dynamic relaxation method (DR) and successfully applied it to the solution of planar frames and plate structures. Barnes [12,13] and W.J. Lewis et al. [14] applied it to the analysis of cable network and spatial membrane structures. S. Chen [15] proposed two calculation formulas for the time step and damping coefficient used in the calculation of the dynamic relaxation method. LU Jian-Heng [16] established a functional relationship among time step, node damping coefficient, and node virtual mass.

For the force finding problem of a tensegrity structure, Pellegrino and Calladine [17–19] proposed an equilibrium equation between the internal force vector and external node force vector, which neglects the elastic characteristics of the structure and change of configuration. The relative advantages and disadvantages of each kind of method are listed in Table 1.

Table 1. Comparison of advantages and disadvantages of different methods.

Method	Elasticity Modulus and Section Parameters Considered	Speed for Finding Reasonable Prestress	Calculation Speed of Economic Cross-Section	Calculation Accuracy	Calculation Speed
force density	no	good	good	not good	good
dynamic relaxation	yes	not good	not good	good	not good
equilibrium matrix theory	no	good	good	not good	good

Combining the cable dome form-finding method with finite element software can complete the cable dome prestressing design more quickly and accurately. Pagitz [20] proposed an iterative form-finding method for any tensioned integral structure with determined prestressing and external forces based on the minimum potential energy principle to achieve an optimal topology by adjusting the lengths of the cable-bars. However, this method requires prior knowledge of the cross-sectional areas of the components. Kai-Uwe [21] introduced a form-finding method based on adaptive stiffness matrix regularization iteration and a parameter update strategy, and its robustness was verified through 2D and 3D examples. However, this method requires knowledge of the internal force distribution. Neither of these methods conforms to engineering application scenarios. In 2007, Li Hongyu and Liu Xiliang [22] proposed the initial displacement disturbance method, which obtained the feasible prestressing distribution relationship of cable dome structures by applying appropriate small displacement disturbance to the finite element truss element model of the cable dome. Its core idea is similar to the pretension springback method proposed by Xiang XA [23] in 2019. Due to the significant difference between the disturbance method and the actual construction process, there is a lack of in-depth literature on the refined application research in the design field. In 2023, Wang Hong and Guo Yanlin, et al. proposed a target position forming analysis method for calculating the initial configuration, which overlooks the changes in component internal forces and sectional stresses during the iterative form-finding process.

This paper relies on the fundamental ideas and principles of the force disturbance method and aims to address the prestressing design problem of cable dome structures with determined load conditions and target configurations. A new structural design method is proposed to calculate the internal prestressing system of cable domes while synchronizing the section design and initial configuration design. The analysis and calculation procedures are established, and corresponding software is developed based on a finite element software

platform. Finally, the effectiveness and practicality of this method are validated through numerical examples.

2. Design Method Based on Minor Perturbation Method

2.1. Fundamental of Minor Perturbation Method

For a statically stable cable dome with certain geometric configuration and boundary constraint, there is a general equilibrium force system inside the structure under pretension load and gravity load. Gravity load is a relatively certain external load, and the pretension load is an artificially applied variable load. Considering that the change of prestress load obviously affects the bearing capacity and stiffness of the structure, it can be assumed that it is a perturbation load.

In theory, behavior characteristics of a system can be understood by observing, analyzing, and comparing the response of the system before and after introducing a perturbation. Originating from this idea, Force Perturbation theory holds that, when facing certain force perturbations that do not obviously change structure configuration within certain boundary constraints, a certain internal force system conforming to the original geometric configuration will come into being to resist the deformation of the structure, and the proportional relationship between the internal forces of each component is also relatively stable. This concept has been proven to be applicable to the process of finding the proportional relationship between internal forces of cables and the structure of the strut.

By extending the above theory into the theory field of elastic cable dome structure, it will inevitably lead to the conclusion that, when applying a pretension force perturbation on any group of cables inside the cable dome structure, based on the stiffness characteristics of the structure itself, a stable internal force system conforming to basic topological characteristics will come to being. The essence of the theoretical conclusion is the development of the node force balance theory considering the distribution characteristics of structural stiffness.

2.2. Determination of Reasonable Prestress Level

Based on the above theory, for a symmetric numerical cable dome simulated with truss elements, with geometric configuration and boundary constraints predetermined, both structural internal force systems under gravity load and unit force perturbation applied to a certain group of cables can be obtained, respectively.

The latter is multiplied by a scaling factor, then the mechanical effects by both loads are mathematically added to obtain the combined internal force system (tension is positive and pressure is negative). Obviously, with the gradual increasing of the scaling factor from 0, the perturbation and the corresponding internal force system also increase accordingly, and the combined internal force in each cable of the dome structure changes from pressure to tension successively. When the internal forces in all cables become just tension and those of all bars are pressure, the combined internal force system conforming to the mechanical composition idea of a cable dome structure is obtained.

The corresponding scaling factor is now the lowest applicable scaling factor, and obviously the tension in each cable is relatively low. This paper defines the combined internal forces stated as a reasonable mechanical state and the pretension internal force system as a reasonable internal force system.

In the working state of a cable dome structure, there exists a generalized force balance relationship composed of the boundary constraints of the outermost ring, gravity loads, and the prestress system induced by tension. According to the classical theory of nodal equilibrium, the comparison of internal forces induced in the components mainly depends on the spatial topological geometric relationships of each component.

Therefore, for a cable dome with a certain configuration, the internal force system under gravity loads can be determined, as well as the internal force system under the prestressing. By mathematically comparing the latter with the former and scaling the latter, the resultant internal force system can be obtained by superimposing the two values mathematically (where tension is represented as positive values and compression as negative values). When the internal forces in the individual elements are tension and the forces in the bar elements are in compression, the internal force system conforming to the mechanical composition principle of the cable dome structure is obtained. Currently, the scaling coefficient and tension in the individual elements is relatively low. In this paper, this state is defined as a relatively reasonable prestress level. Under this relatively low resultant internal force system, the cross-sectional areas of the components are adjusted in design to make the sectional stresses of each component close to the control stress. As a result, the obtained cross-sections will be smaller, and the overall material consumption will be reduced.

Load conditions and prestress states are two key states in the installation and utilization of cable dome structures. The distinction lies in the load condition encompassing not only all structural self-weight inherent in the prestress state but also additional loads from roofing materials and live loads. However, the pretension internal force system inherits and equates to that of the prestress state. The resultant internal force system that meets the feasibility criteria for cable dome structures, as previously described, is the one under load conditions.

In the two states (hereinafter referred to as Combination 1 and Combination 2), the former state results in maximal tensile forces in the inclined and hoop cables of the cable dome, while the latter state places maximal forces on ridge and stabilizing cables. Therefore, the aforementioned resultant internal force system should encompass the resultant force systems from two conditions. For each component within these two resultant force systems, there is a corresponding internal force value. In calculating the economic section, this paper adopts the approach of selecting the larger of the absolute values of the corresponding elements from the two force systems to formulate an effective resultant force system. This method essentially employs an envelope design approach.

2.3. Determination of Initial Configuration

After updating the model by the aforementioned prestress distribution and cross-section, the deformation values of new structure and final configuration under load Combination 3 can be determined. Then, the paper adjusts the model configuration by the values reversely until the final configuration under the Combination 3 load has almost no deference from the target configuration.

3. Design Process

This paper divides the resolution of the pretension internal force system (also called force-finding module) and the initial configuration (also called form-finding module) into two consecutive steps. The design flow is shown in Figure 1 in which force-finding module is enclosed by red dotted line.and another blue line.

$$\boldsymbol{F}(i) = \begin{cases} \max(\boldsymbol{F}_a(i), \boldsymbol{F}_b(i)) & \text{Suitable for cable} \\ \min(\boldsymbol{F}_a(i), \boldsymbol{F}_b(i)) & \text{Suitable for strut} \end{cases} \tag{1}$$

$$\boldsymbol{ES}(i) = \begin{cases} \max(\boldsymbol{ES}_a(i), \boldsymbol{ES}_b(i)) & \text{Suitable for cable} \\ \min(\boldsymbol{ES}_a(i), \boldsymbol{ES}_b(i)) & \text{Suitable for strut} \end{cases} \tag{2}$$

where $\boldsymbol{F}_{con}$ is the control stress vector; $\boldsymbol{I}$ is the identity vector; *mean* is the vector averaging operator, and *abs* is the absolute value operator; *abs*(*mean*($\boldsymbol{ES./F}_{con}$-I)) is the target values for the force-finding module; 5% is the design target boundary value set in this paper; $\Delta\boldsymbol{D}_{z0}$ and $\Delta\boldsymbol{D}_{l0}$ are vectors representing the initial vertical and radial deformation values of the structure's nodes, respectively, also referred to as the initial shape basic compensation vectors in subsequent sections. *m1i* and *m2i* are the proportion coefficients of shape basic compensation, with allowable values ranging from 0 to 2.0. $\Delta\boldsymbol{D}_z$ and $\Delta\boldsymbol{D}_l$ are the vectors of deformation differences between the final and target shapes of the structure after shape correction under combined load case 3. $\Delta\boldsymbol{D}_{lim}$ is the vector of deformation difference limits between the final and target shapes.

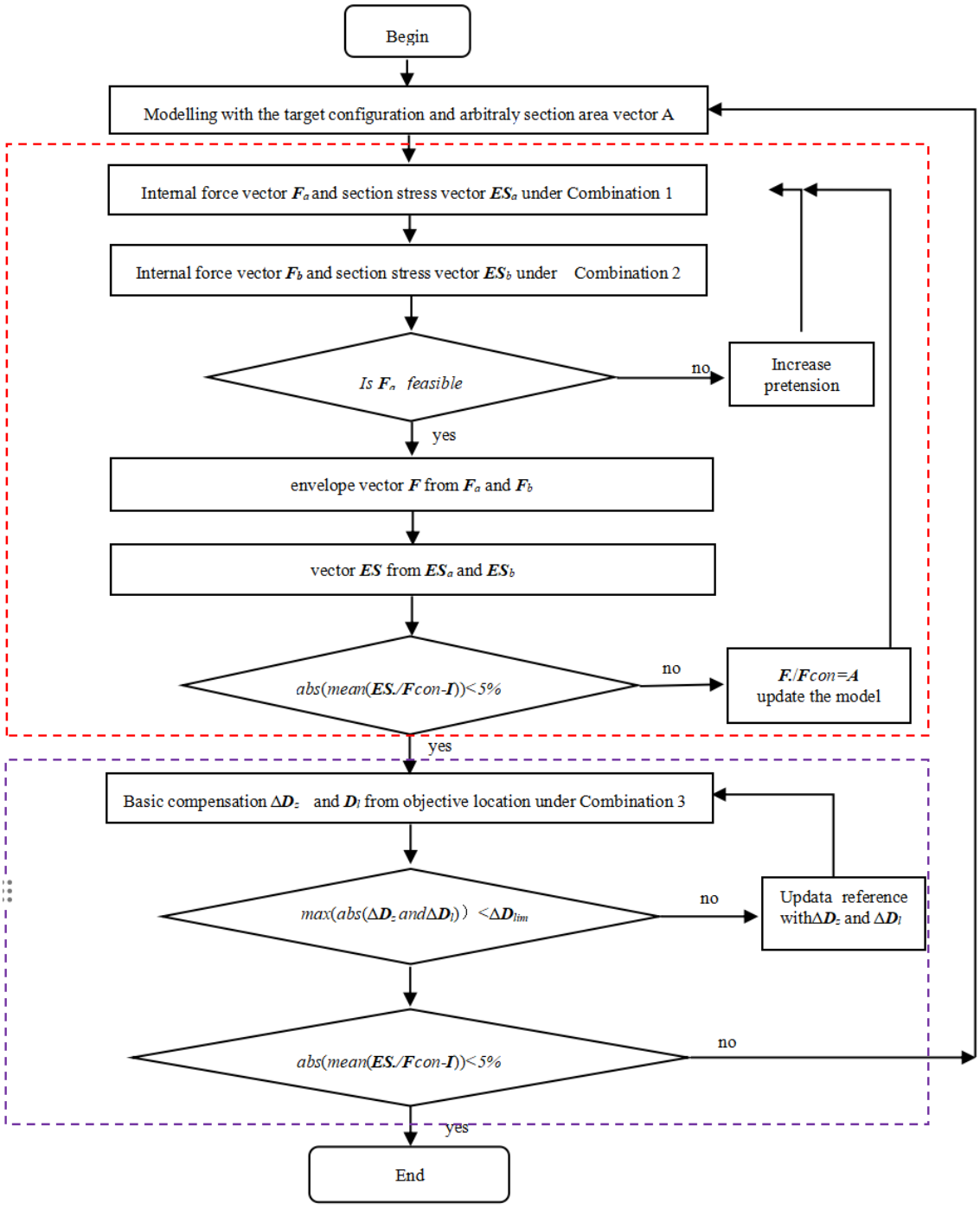

Figure 1. Design flow chart.

4. Case Study

4.1. Case 1

Academician Dong Shilin proposed the open-type bulged honeycomb four-strut Type III cable dome structure, which has distinct features among the numerous new cable dome systems that have emerged in recent years. This structure is statically indeterminate. The example structure has an outer diameter of 100 m (Figure 2) and an inner diameter of 40 m. It features a 16-sided, double-layered ring cable with radii of 27 m and 42.5 m, and a thickness-span ratio of 1/20. Geometrically, it is divided into eight symmetrical modules, each with a circumferential angle of 1/8 of a circle (i.e., 45°). Within a single module, the internal honeycomb angle a is 13.5°, and the external angle b is 22.5°, which are 0.3 and 0.5 times the 45° sector, respectively. The aforementioned dimensions are also the target shape of this case study, with the initial finite element model established based on this shape. In Figure 2, HS1/HS2 represent different ring cables at the lower level and WS1/WS2/WS3/WS4 represent circumferential stabilizing cables at the upper level. XS1/XS2 represent inner and outer radial inclined cable respectively and JS1/JS2/JS3/JS4 represent different radial ridge cables while CG1-1/CG1-2/CG2-1/CG2-2 represent bar stays.

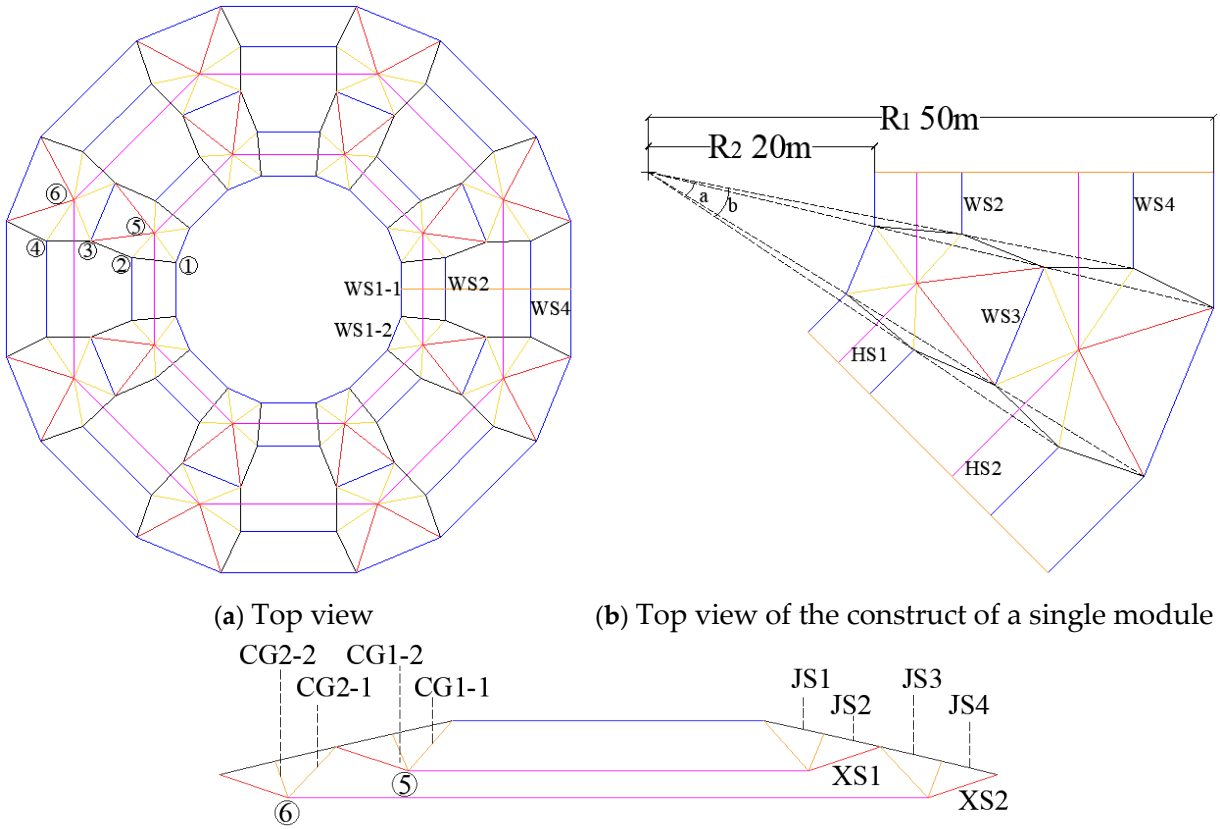

(**a**) Top view (**b**) Top view of the construct of a single module

(**c**) Front view

Figure 2. Structure diagram of drum honeycomb cable dome.

The cables are made of high-vanadium steel with an elastic modulus of 1.6×10^5 MPa and a design strength of 1670 MPa; the struts are made of Q345B steel with an elastic modulus of 2.0×10^5 MPa and a design strength of 315 MPa. In the $\boldsymbol{F}_{con}$ control stress vector, the control stress for cable elements is uniformly set at 400 MPa, and for strut elements at −50 MPa. In the $\Delta \boldsymbol{D}_{lim}$ deformation difference limit vector, all values are uniformly set to ±10 mm. The roof is subject to an additional permanent load of 0.3 kN/m^2

and a live load of 0.5 kN/m^2, which is converted into concentrated forces applied at the ridge cable nodes. The self-weight of the cable dome structure is multiplied by a factor of 1.5 to account for the weight of the clamps.

The pretension force is achieved by applying a negative thermal load to the outermost inclined cable XS2. All component cross-sectional areas are uniformly input with an arbitrary value of 10,000 mm^2. Tables 2–4 show the main data of the calculation process.

Table 2. The first loop iteration process data for the force-finding module for case 1.

No.	Rod	A_1 (mm^2)	ES_1 (MPa)	A_2 (mm^2)	ES_2 (MPa)	A_3 (mm^2)	ES_3 (MPa)	A_4 (mm^2)	ES_a (MPa)	ES_b (MPa)	ES_4 (MPa)	F_b (kN)
1	JS1	10,000	60	1489	286	1062	385	1021	124	**403**	**403**	411
2	JS2	10,000	69	1718	288	1233	386	1186	101	**403**	**403**	478
3	JS3	10,000	172	4294	261	2802	378	2643	337	**402**	**402**	1062
4	JS4	10,000	214	5338	261	3484	378	3289	321	**403**	**403**	1325
5	CG1-1	10,000	−18	3696	−33	2412	−47	2268	−35	**−50**	**−50**	−113
6	CG1-2	10,000	−14	2704	−42	2274	−44	2003	**−51**	−11	**−51**	−102
7	XS1	10,000	40	989	292	720	387	694	**401**	282	**401**	278
8	CG2-1	10,000	−91	18,254	−40	14,576	−48	14,104	**−50**	−32	**−50**	−705
9	CG2-2	10,000	−40	7915	−43	6770	−50	6830	**−51**	−29	**−51**	−348
10	XS2	10,000	211	5285	332	4445	385	4360	**395**	258	**395**	**1722**
11	WS1-1	10,000	129	3237	290	2343	386	2254	100	**404**	**404**	911
12	WS1-2	10,000	106	2640	265	1749	378	1650	344	**402**	**402**	663
13	WS3	10,000	112	2790	292	2034	386	1960	88	**403**	**403**	790
14	WS4	10,000	33	829	296	611	387	589	5	**402**	**402**	237
15	WS5	10,000	132	3308	262	2165	374	2017	256	**401**	**401**	809
16	HS1	10,000	100	2498	270	1682	387	1622	**401**	338	**401**	650
17	HS2	10,000	523	13,069	333	10,850	393	10,631	**401**	262	**401**	4263

Table 3. The first loop iteration process data for the form-finding module for case 1 (unit: mm).

Direction \ Control Point	1	2	3	4	5	6
Basic compensationΔD_{l0}	39.08	55.97	76.21	91.61	59.39	79.04
Basic compensation ΔD_{z0}	296.51	306.99	325.05	312.79	316.49	334.47
Effective compensation $-1.00\Delta D_{l0}$	39.08	55.97	76.21	91.61	59.39	79.04
residual error ΔD_{lmin}	0.09	−0.06	−0.18	−0.11	−0.52	0.09
$-1.00\Delta D_{l0}$-ΔD_{lmin}	−39.18	−55.91	−76.03	−91.51	−58.87	−79.12
Effective compensation $-1.05\Delta D_{z0}$	311.34	322.34	341.31	328.43	332.32	351.19
residual error ΔD_{zmin}	3.85	2.55	1.68	1.83	1.04	−3.80
$-1.05\Delta D_{z0}$-ΔD_{zmin}	315.19	324.88	342.98	330.25	333.36	347.39
ΔD_l	1.31	2.49	3.85	3.77	3.05	3.87
ΔD_z	−3.37	−4.36	−5.27	−6.16	−2.39	−6.46

Table 4. The second loop iteration process data for the force-finding module for case 1.

No.	Rod	A_1 (mm^2)	ES_1 (MPa)	A_2 (mm^2)	ES_2 (MPa)	A_3 (mm^2)	ES_a (MPa)	ES_b (MPa)	ES_3 (MPa)	F_b (kN)	$(A_3 - A_1)/A_1$
1	JS1	1021	285	1068	382	1018	120	**399**	**399**	406	−0.27%
2	JS2	1186	287	1240	382	1183	97	**399**	**399**	472	−0.28%
3	JS3	2643	261	2818	376	2642	334	**398**	**398**	1052	−0.03%
4	JS4	3289	261	3503	376	3288	317	**398**	**398**	1309	−0.03%
5	CG1-1	2268	−33	2425	−47	2268	−35	**−50**	**−50**	−113	0.02%
6	CG1-2	2003	−42	2280	−49	2047	**−50**	−9	**−50**	−102	2.15%
7	XS1	694	292	723	385	695	**400**	280	**400**	278	0.07%
8	CG2-1	14,104	−40	14,627	−48	14,109	**−50**	−32	**−50**	−705	0.04%
9	CG2-2	6830	−43	6790	−50	6829	**−50**	−28	**−50**	−341	−0.02%
10	XS2	4360	331	4460	384	4359	**393**	255	**393**	**1713**	−0.01%
11	WS1-1	2254	290	2357	384	2255	94	**399**	**399**	900	0.03%
12	WS1-2	1650	265	1759	376	1649	341	**398**	**398**	656	−0.05%
13	WS3	1960	292	2046	384	1958	83	**399**	**399**	781	−0.12%
14	WS4	589	295	615	383	587	1	**399**	**399**	234	−0.36%
15	WS5	2017	262	2177	371	2017	252	**397**	**397**	801	0.02%
16	HS1	1622	270	1689	385	1622	**400**	335	**400**	649	0.01%
17	HS2	10,631	332	10,888	391	10,628	**401**	260	**401**	4262	−0.03%

The force-finding module computation is performed first. As can be seen from Table 2 above, after three iterations the maximum stresses (ES_4) in the cable and strut elements are around 400 MPa and −50 MPa, respectively, with the design target value reduced to 0.47%, which is below the limit value of 5%. Consequently, the operation of the force-finding module is ceased. The cross-sectional areas of the components are as shown in column A4 of Table 2, with the corresponding prestressed state component stresses and internal forces displayed in the last two columns of the table. By applying the negative thermal load obtained from the final iteration step (corresponding to a pretension force of 1722 kN) to the outer inclined cable XS2, stress distribution contour maps under two combinations are obtained (Figure 3). These maps show complete agreement with the corresponding data in Table 2, where the inclined cables and ring cables under Combination 1, and the ridge cables and stabilizing cables under Combination 2, all have sectional stresses around the control stress of 400 MPa, indicating good economic efficiency.

Building upon the inherited cross-sectional areas and pretension thermal loads, the structural configuration under Combination 3 is verified. Displacements for six control nodes (Figure 4) are measured in the vertical and radial directions (Table 3, first two rows of data, indicating deviation from the initial configuration, also known as the basic compensation vector). The maximum vertical rise is 334.47 mm, and the maximum horizontal radial displacement is 79.04 mm. The form-finding module calculation commences with key data presented in Table 3. It is evident that, when the coordinates of each node of this tensegrity honeycomb dome structure example deviate from the target configuration according to the data in rows 5 and 8, respectively, under the effects of load Combination 3, the maximum absolute displacements of the deformed structure from the target configuration are 3.87 mm and −6.46 mm, respectively, which are less than the allowable deformation difference limit of 10 mm. The initial and target configurations of the form-finding structure are depicted by the solid red and dashed black lines in Figure 5, respectively.

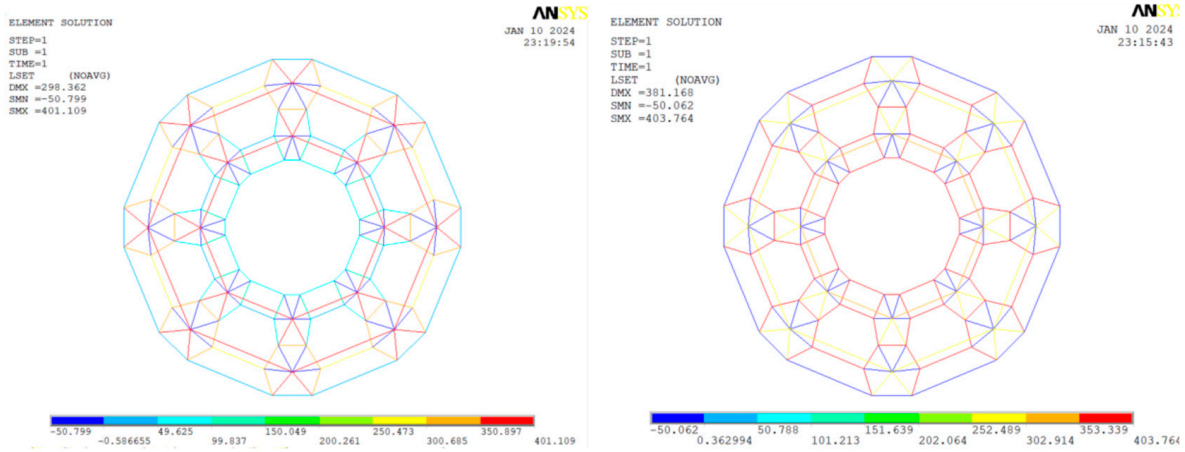

(**a**) Combination 1 (**b**) Combination 2

Figure 3. Axial stress contour maps of components under two combinations for case 1.

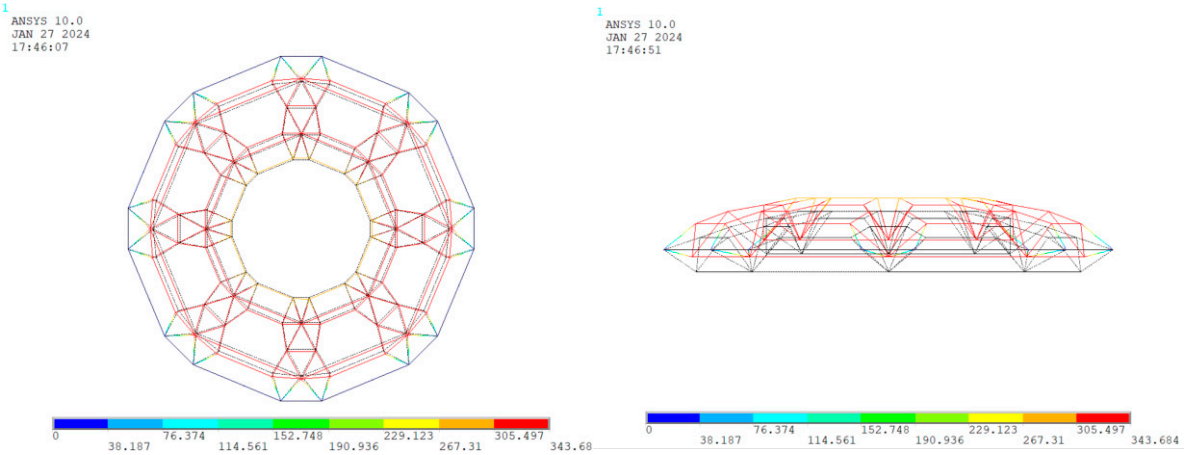

(**a**) Top view (**b**) Side view

Figure 4. Structural deformation contour map for Combination 3 (magnified 5 times) for case 1.

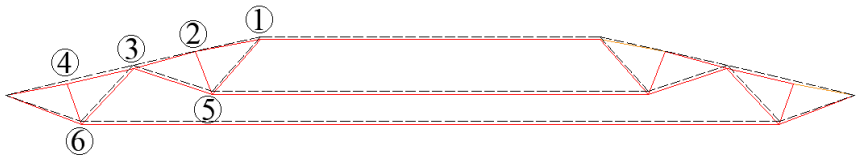

Figure 5. Comparison of the initial and target configurations for case 1 after form-finding (①–⑥ represnt control points in dome for deformation monitoring).

Following the first loop form-finding process, the nodes of the adjusted cable dome (excluding the outermost ring nodes) settled by varying amounts between 315–347 mm, with minor changes occurring in the angular relationships between components. Under the original negative temperature load, the maximum tensile stresses within the components under Combinations 1 and 3 experienced a slight overall decrease (approximately 20 MPa). Consequently, in accordance with the design process requirements, a second loop of iterative calculations for the force-finding module was conducted based on the current structural configuration and component cross-sections. The data from this computational process are shown in Table 4. The calculations converged after two iterations. By comparing the final columns of data in Tables 2 and 4, it is observed that, aside from a 2.15% increase in the cross-sectional area of the sensitive component CG1-2, there were virtually no

changes to the cross-sectional areas or prestress levels of the other components. The cross-sectional areas, stress levels, and configurations of the structure are now very stable, and the calculations meet convergence criteria, terminating the program's operation and completing the design. The theoretical steel usage is calculated at 13.52 kg/m^2 (excluding the support ring beams).

Adjustments to angles a and b resulted in changes to the steel usage of the structure, as shown in Table 5. It is evident that the steel usage per unit area of the structure monotonically increases with the incremental enlargement of angles a and b. This is primarily due to the large number and cross-sectional area of the struts in this system, which account for a significant proportion of the total steel usage, making angles a and b the main influencing factors on the overall steel consumption.

Table 5. Economic steel consumption statistics table for structures under different conditions of a and b (Unit: kg/m^2).

a \ b	**13.5°**	**18.0°**	**22.5°**	**27.0°**	**31.5°**	**36.0°**
9.0°	12.03	10.14	11.32	12.73	13.07	14.01
13.5°	-	13.46	13.52	12.45	13.84	15.85
18.0°	-	-	15.36	15.95	16.72	17.93
22.5°	-	-	-	18.15	17.83	18.76
27.0°	-	-	-	-	20.07	20.41
31.5°	-	-	-	-	-	24.61

Based on empirical findings, when the single-unit control stress in this case is set at 420 MPa, the post-shape-finding module operation typically results in single-unit stress levels fluctuating around 400 MPa, thereby obviating the need for a second iteration of calculations.

4.2. Case 2

Figure 6 depicts a 30-m span Geiger-type cable dome with an outer diameter of 30 m, an inner diameter of 6 m, and a thickness-span ratio of 1: 10. Material properties, control stress levels, load values, and loading methods are consistent with Case Study 1. Computational process data are presented in Table 6. the Letters HS1/HS2 and so on represent the same meaning as in the case 1 and ①–⑥ represnt the key point in the dome for deformation monitoring.

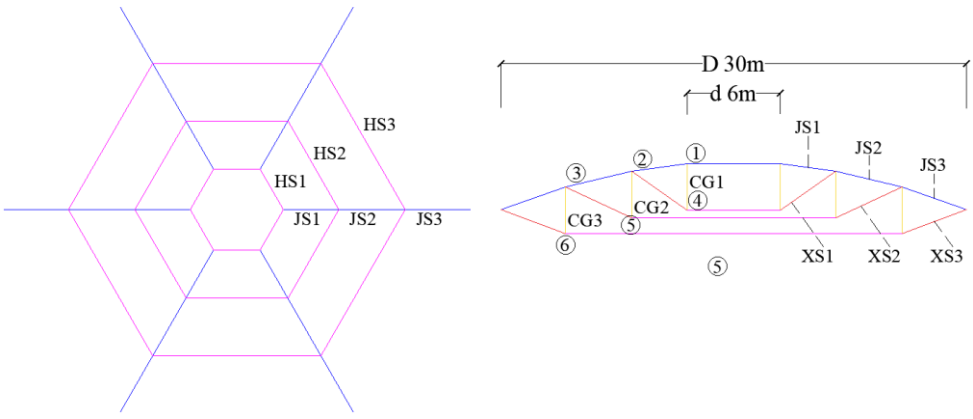

(**a**) Top view (**b**) Side view

Figure 6. Construction of Geiger-type cable dome calculation case.

Table 6. The first loop iteration process data for the force-finding module.

No.	Rod	A_1	ES_1	A_2	ES_2	A_3	*ES2*	*A3*	*ESa*	*ESb*	*ES4*	F_b
		(mm^2)	(MPa)	(mm^2)	(MPa)	(mm^2)	(MPa)	(mm2)	(MPa)	(MPa)	(MPa)	(kN)
1	JS1	10,000	17	426	225	240	394	236	26	**402**	**402**	95
2	JS2	10,000	23	583	203	295	392	288	39	**401**	**401**	115
3	JS3	10,000	44	1098	171	468	389	455	237	**401**	**401**	182
4	XS1	10,000	7	167	137	57	379	54	223	**400**	**400**	22
5	XS2	10,000	25	613	174	266	373	247	**403**	259	**403**	100
6	XS3	10,000	80	2009	204	1031	400	1042	**378**	197	**378**	**394**
7	CG1	10,000	−3	520	−21	223	−48	213	−28	**−50**	**−50**	−11
8	CG2	10,000	−9	1782	−25	893	−49	879	**−48**	−30	**−48**	−42
9	CG3	10,000	−26	5255	−26	2768	−49	2711	**−49**	−24	**−49**	−133
10	WS1	10,000	17	424	225	238	395	234	2	**402**	**402**	94
11	HS1	10,000	6	145	137	50	379	47	222	**400**	**400**	19
12	HS2	10,000	22	554	176	244	363	221	**407**	263	**407**	90
13	HS3	10,000	75	1884	205	963	411	986	**381**	199	**381**	376

The initial step involved force-finding module computations. As indicated in the table above, after three iterations, the maximum stresses for the cables and struts were approximately 400 MPa and −50 MPa, respectively, with the design target value reduced to 1.53%, which is below the limit value of 5%, leading to the termination of the force-finding module. The cross-sectional areas of the components are as listed in column A4 of the said table, with corresponding prestress state component stresses and internal forces presented in the last two columns of the same table. The negative temperature load obtained from the last iteration step (corresponding to a pretension force of 394 kN) was applied to the outer ring inclined cable XS3, resulting in the sectional stress distribution cloud maps under two combinations as shown in Figure 7. These match perfectly with the corresponding data in Table 5, where the section stresses of the inclined cables and hoop cables under Combination 1, as well as the ridge cables and stabilizing cables under Combination 2, are all around the control stress of 400 MPa, indicating favorable economic efficiency.

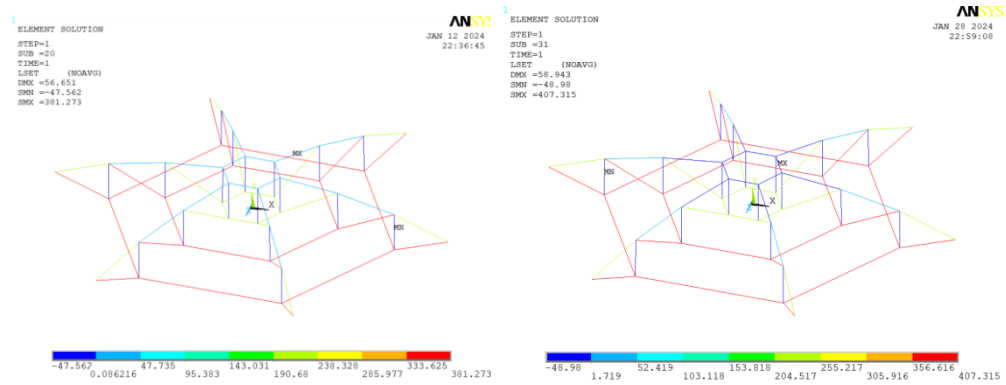

(**a**) Combination 1 (**b**) Combination 2

Figure 7. Axial stress contour maps of components under two combinations.

Building upon the previously defined cross-sectional areas and pretension temperature loads, the structure's configuration under Combination 3 was validated (Figure 8).

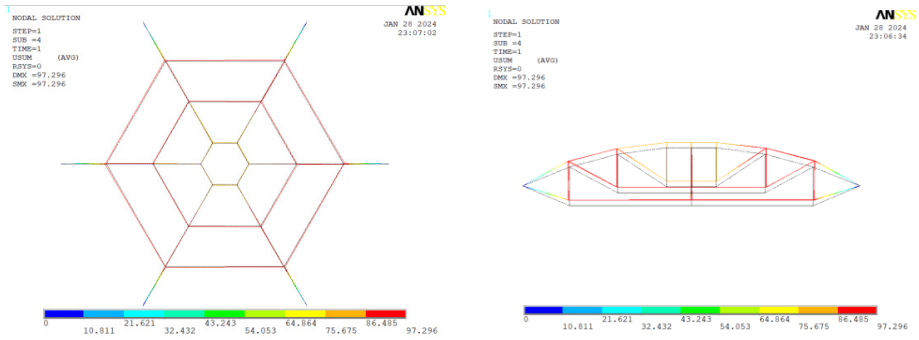

Figure 8. Structural deformation contour map for Combination 3 (magnified 5 times).

Deformation values at control nodes, both vertical and radial, were obtained as basic compensation vectors. Then, the first loop form-finding process commences and minor changes occurred in the angular relationships between components, resulting in slight fluctuations in component stresses and internal force systems. In compliance with the design workflow, a second loop force-finding module iteration computations was conducted until meeting convergence criteria.

5. Conclusions

The practical application of the force perturbation method in the field of tensegrity dome structures has been extensively studied through theoretical exposition and case study verification. The following conclusions are drawn:

(1) Based on the basic principles of the force perturbation method, a design methodology for the internal force system and component cross-sections of tensegrity dome structures was proposed, targeting economical material usage and feasible prestress force distribution. This was done under predetermined target configurations and load conditions. An analysis workflow was established, and corresponding software was developed.

(2) The program was applied to the structural analysis and design of a Honeycomb tensegrity dome and a Geiger-type tensegrity dome. The results validate the proposed design methodology as conceptually sound, well organized, and simple to execute, with the derived data satisfying target requirements.

In summary, the approach presented in this paper can aid engineers in the rapid design of tensegrity domes that are material-efficient, with a suitable level of prestress and feasible initial configurations. In addition to the sphere of tensegrity domes, this method also has significant implications for other tensile structural systems.

Author Contributions: Software, H.Z.; Investigation, H.Z. and D.Y.; Data curation, B.S. and F.Z.; Writing—original draft, H.Z.; Writing—review & editing, F.F. All authors have read and agreed to the published version of the manuscript.

Funding: This research was funded by Henan Province Science and Technology Research, China, grant number 1000; research and application of prefabricated recycled ceramic foam concrete self-insulated wall panel technology, Henan Province Housing and Urban Rural Construction Science and Technology Plan Project K-2320.

Data Availability Statement: The original contributions presented in this study are included in the article. Further inquiries can be directed to the corresponding author.

Conflicts of Interest: Bo Si and Deqing You were employed by Beijing Building Construction Research Institute Co., Ltd. The remaining authors declare that the research was conducted in the absence of any commercial or financial relationships that could be construed as a potential conflict of interest.

References

1. Fuller, R.B. *Synergetics: Explorations in the Geometry of Thinking*; Scribner: New York, NY, USA, 1982.
2. Tibert, A.G.; Pellegrino, S. Review of Form-Finding Methods for Tensegrity Structures. *Int. J. Space Struct.* **2011**, *26*, 241–255. [CrossRef]
3. Linkwitz, K.; Schek, H.J. Einige Bemerkungen zurBerechnung von vorgespannten Seilnetzkonstruktionen. *Ing. Arch.* **1971**, *40*, 145–158. [CrossRef]
4. Schek, H.J. The force density method for form finding and computation of general networks. *Comput. Methods Appl. Mech. Eng.* **1974**, *3*, 115–134. [CrossRef]
5. Gründig, L. Minimal surfaces for finding forms of structural membranes. *Comput. Struct.* **1988**, *30*, 679–683. [CrossRef]
6. Zhang, J.Y.; Ohsaki, M. Adaptive force density method for form-finding problem of tensegrity structures. *Int. J. Solids Struct.* **2006**, *43*, 5658–5673. [CrossRef]
7. Tran, H.C.; Lee, J. Advanced form-finding of tensegrity structures. *Comput. Struct.* **2010**, *88*, 237–246. [CrossRef]
8. Miki, M. Extended force density method for form finding of tension structures. *J. Int. Assoc. Shell Spat. Struct.* **2010**, *51*, 291–303.
9. Metro, R.; Maurin, B.; Vassart, N. Density Methods Applied to Form Finding of Initially Stressed Systems. In *Novel Approaches in Civil Engineering*; Frémond, M., Maceri, F., Eds.; Springer: Berlin/Heidelberg, Germany, 2004; pp. 341–350. ISBN 978-3-540-41836-8.
10. Maurin, B.; Motro, R. The surface stress density method as a form-finding tool for tensile membranes. *Eng. Struct.* **1998**, *20*, 712–719. [CrossRef]
11. Day, A.S.; Bunce, J.H. Analysis of cable networks by dynamic relaxation. *Civ. Eng. Public Work. Rev.* **1970**, *4*, 383–386.
12. Barnes, M.R. Applications of dynamic relaxation to the design of cable, membrane and pneumatic structures. In Proceedings of the Second International Conference on Space Structures, Guildford, UK, 11 September 1975.
13. Barnes, M.R. Form Finding and Analysis of Tension Structures by Dynamic Relaxation. *Int. J. Space Struct.* **1999**, *14*, 89–104. [CrossRef]
14. Lewis, W.J.; Shan, J. Numerical modeling of the non-linear static response of clad cable net structure. *Comput. Struct.* **1990**, *35*, 15–22. [CrossRef]
15. Chen, S. The efficiency of dynamic relaxation methods in static analysis of cable structures. *Chin. J. Appl. Mech.* **2002**, *19*, 34–37.
16. Lu, J.-H. Parameters Simplification of Dynamic Relaxation Method in Form Finding of Prestressed Nets and Membranes. *J. Huazhong Univ. Sci. Technol.* **2006**, *23*, 82–84.
17. Calladine, C.R. Buck minster Fuller Tensegrity structure and Clerk Maxwell's rules for the construction of stiff frames. *Int. J. Solids Struct.* **1978**, *14*, 161–172. [CrossRef]
18. Pellegrno, S.; Calladine, C.R. Matrix analysisof staticallly and kinematically indeterminate frame work. *Int. J. Solids Struct.* **1986**, *22*, 409–428. [CrossRef]
19. Pellegrno, S. Structural Computation with the Singular Value Decomposition of Equilibrium Matrix. *Int. J. Solids Struct.* **1993**, *30*, 3025–3035. [CrossRef]
20. Pagitz, M.; Tur, J.M. Finite element based form-finding algorithm for tensegrity structures. *Int. J. Solids Struct.* **2009**, *46*, 3235–3240. [CrossRef]
21. Bletzinger, K.-U.; Ramm, E. A General Finite Element Approach to the form Finding of Tensile Structures by the Updated Reference Strategy. *Int. J. Space Struct.* **1999**, *14*, 131–145. [CrossRef]
22. Li, H.; Liu, X. Preliminary study on the new method of prestressed design of cable dome. In Proceedings of the 7th National Symposium on Modern Structural Engineering, Hangzhou, China, 20 July 2007; pp. 1038–1041.
23. Xiang, X.A.; Feng, Y. A New Method of Determining the Initial Prestress Distribution of Cable Domes- the pretension and Rebound Method. *Eng. Mech.* **2019**, *36*, 45–52.